P. Freymuth, Int. Journal of Design & Nature. Vol. 1, No. 2 (2007) 87–99

OSCILLATING AERO-WING MODEL IN THE QUASI-STEADY DOMAIN – A REFERENCE FOR SUSTAINED ANIMAL FLIGHT AND MICRO AIR VEHICLES

P. FREYMUTH
Department of Aerospace Engineering Sciences, University of Colorado, USA.

ABSTRACT

An oscillating aero-wing operating in pitch and plunge in the quasi-steady domain for lift and thrust generation is presented and analyzed. The model may serve as a reference of comparison for sustained forward propulsion of birds, insects and micro air vehicles. It turns out that the propulsive efficiency of the aero-wing cannot be maximized with respect to the Strouhal number since this number is fixed by the drag-to-lift requirements of an overall system. This is in contrast to the liftless propulsion by a hydro-wing in water. The remaining criteria for aero-propulsion are the minimization of the drag-to-lift ratios of the aero-wing and of the overall flight system. Some other current issues of aero-propulsion are discussed for model support and refinement.
Keywords: aerodynamic propulsion, bio-aerodynamics, flow visualization, propulsive efficiency.

1 INTRODUCTION TO THE AERO-WING MODEL

Birds, insects and micro air vehicles (MAVs) rely on the complex aerodynamics of flapping wings to keep the animal or vehicle aloft and to thrust it forward during sustained flight [1].

To model basic aero-propulsion without the complexity of natural flight, consider a single rectangular wing in a downstroke at steady speed v_0 and facing a steady horizontal wind at steady speed U_0 as in Fig. 1. Given a proper angle of attack α_r with respect to the relative wind of speed

$$U_r = \left(U_0^2 + v_0^2\right)^{1/2}, \tag{1}$$

the wing can generate a lift S which balances the gravity force of the entire system such that

$$S = m_0 g, \tag{2}$$

where m_0 is the mass of the entire system and g is the gravitational constant. Furthermore, the wing needs to generate a thrust T to balance the drag D_b of the system body such that

$$T = D_b. \tag{3}$$

The model assumes a downstroke of the wing from a top position $+h_a$ to a bottom position $-h_a$. After the downstroke is finished, the wing is quickly retracted in an upstroke at a zero angle of attack so as to generate no lift and low drag and the entire cycle of downstroking and upstroking is periodically repeated. Neglecting the upstroke time compared to the lift and thrust generating downstroke, the frequency of wing oscillation f is

$$f = \frac{v_0}{2h_a}. \tag{4}$$

In many animals, downstroke and upstroke require similar time durations and this slight modification of the model will be considered in Section 4.1. Neglecting unsteadiness during stroke reversals, the aero-wing model is treated as quasi-steady. This allows the use of classic wing theory and experiment for wing force determination and has recently been presented for a hydro-wing as a reference model of aquatic liftless propulsion [2].

ISSN: 1744-3687 (paper format), ISSN: 1744-3679 (online), http://journals.witpress.com
DOI: 10.2495/D&N-V1-N2-87-99

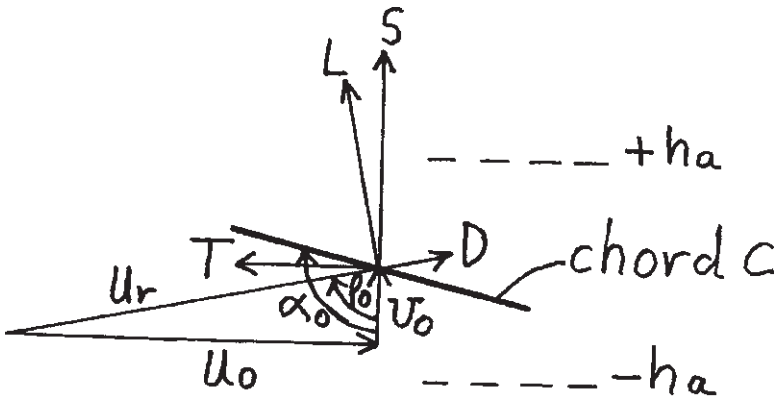

Figure 1: Sketch of a wing during downward traverse from top position $+h_a$ to bottom position $-h_a$ at constant lateral speed v_0.

More complex models of animal flight have been considered for a long time with limited success. For a critical historical review of these theories, the reader is referred to [3]. For the most recent progress in the computational analysis of complex unsteady wing flows with application to MAVs and birds, the reader is referred to [4] and [5]. The focus of these analyses is the complex unsteady vortex shedding process. In contrast, the current paper focuses on thrust and lift generation due to quasi-steady vortex stretching. This simplified model may serve as a reference for potentially more realistic but correspondingly more complex models.

2 MODEL CHARACTERISTICS

Several dimensionless quantities characterize the model as follows.

The relative wind subtends an angle φ_0 with the vertical as sketched in Fig. 1 and which is determined by

$$\tan\varphi_0 = \frac{U_0}{v_0} \stackrel{\text{def}}{=} r^{-1}, \tag{5}$$

where r^{-1} is variously termed dimensionless travel speed or advance ratio and where the inverse quantity $r = v_0/U_0$ is sometimes used instead of r^{-1}. It is also common to introduce another related quantity termed the Strouhal number [6] defined by

$$St \stackrel{\text{def}}{=} \frac{2h_a f}{U_0}. \tag{6}$$

Using eqn (4) we can relate in our model the Strouhal number to the dimensionless travel speed by the equivalence

$$St = \frac{v_0}{U_0} = r = \frac{1}{r^{-1}}. \tag{7}$$

The wing leads into the relative wind at an angle of attack α_r determined by

$$\alpha_r = \alpha_0 - \varphi_0, \tag{8}$$

where in Fig. 1 α_0 is the wing angle with the vertical or pitch angle. During the downstroke and due to an angle of attack of the wing α_r, it generates lift L perpendicular to the relative wind and drag D

in the direction of the relative wind as sketched in Fig. 1. These forces can be characterized by the usual force coefficients of lift and drag and which primarily depend on α_r for a given wing as follows.

$$C_L(\alpha_r) = \frac{L}{(\rho/2)U_r^2 cl}, \tag{9}$$

$$C_D(\alpha_r) = \frac{D}{(\rho/2)U_r^2 cl}, \tag{10}$$

where ρ is the air density, c is the chord length and l is the wing span. C_L and C_D also depend on the aspect ratio, the airfoil profile and the Reynolds number $Re = U_r c/\nu$ (ν is the kinematic viscosity of air). C_D and C_L can be obtained from common textbooks on classic aerodynamics [7], except see [1] for the low Reynolds number range of insects. In addition to C_D and C_L, the following force ratios are useful:

$$\frac{D}{L} = \frac{C_D}{C_L}, \tag{11}$$

$$m \stackrel{\text{def}}{=} \frac{T}{S} = \frac{D_b}{m_0 g}. \tag{12}$$

D/L is the drag-to-lift ratio of the wing and m is the body drag-to-upward lift ratio of the system.

3 PERFORMANCE ANALYSIS OF THE AERO-WING

The upward lift force S and horizontal thrust force T generated by the downstroking wing relate kinematically to the lift and drag forces L and D with respect to the relative wind according to Fig. 1:

$$S = L\sin\varphi_0 + D\cos\varphi_0, \tag{13}$$

$$T = L\cos\varphi_0 - D\sin\varphi_0. \tag{14}$$

Therefore,

$$\frac{T}{S} = \frac{D_b}{m_0 g} = m = \frac{L\cos\varphi_0 - D\sin\varphi_0}{L\sin\varphi_0 + D\cos\varphi_0}. \tag{15}$$

Dividing the top and bottom of eqn (15) by $L\cos\varphi_0$ and using eqn (5) yields

$$m = \frac{1}{r^{-1}} \frac{1 - r^{-1}(D/L)}{1 + (1/r^{-1})(D/L)}, \tag{16}$$

or inversely

$$r^{-1} = \frac{1}{m} \frac{1 - m(D/L)}{1 + (1/m)(D/L)}. \tag{17}$$

The propulsive efficiency η of the aero-wing is defined as the ratio of useful power $TU_0 = D_b U_0$, which thrusts the body or vehicle forward, to the power of the wing Sv_0 required for this. In view of this definition and eqns (5), (16) and (17), we find

$$\eta = \frac{D_b}{S}\frac{U_0}{v_0} = mr^{-1} = \frac{1 - r^{-1}(C_D/C_L)}{1 + (1/r^{-1})(C_D/C_L)} = \frac{1 - m(C_D/C_L)}{1 + (1/m)(C_D/C_L)}. \tag{18}$$

The dependence of η on r^{-1} and on C_D/C_L is the same as found for liftless hydro-wing propulsion [2]. As already discussed [2], η has a maximum with respect to r^{-1} at $r^{-1} \simeq 1$ provided $C_D/C_L \ll 1$. Since in aero-propulsion the drag of the body is considerably smaller than lift, i.e. $D_b/S = m$ is considerably smaller than 1, it follows that r^{-1} is considerably larger than 1, of order 5 according to [8]. Since r^{-1} is thus fixed, it cannot be changed to optimize η near $r^{-1} = 1$. In aero-propulsion, the propulsive efficiency is by necessity off-optimum, albeit it may still be respectable.

Example: $r^{-1} = 5$, $C_D/C_L = 1/30$; then according to eqn (18) $\eta = 0.83$, according to eqn (16) $m = 0.17$, and according to [2] $\eta_{\max} \simeq 1 - 2C_D/C_L = 0.93$. Note that the Strouhal number in this example is $St = 1/r^{-1} = 0.2$, a value which agrees with that for many birds in cruise flight [9]. According to [9] the propulsive efficiency should reach its maximum there, but our example shows otherwise. Because in bird propulsion efficiency η must be off-optimum, another optimization principle may still be considered as follows.

Consider a flight system (bird, MAV) of mass m_0 cruising at a design speed U_0. What is the least energy per weight and distance traveled, as required, to thrust the system forward? The required energy per weight and distance traveled is

$$\frac{D_b}{m_0 g \eta} = \frac{m}{\eta} = \frac{1}{r^{-1}} = St = \frac{m + (C_D/C_L)}{1 - m(C_D/C_L)} = \frac{(D_b/S) + (D/L)}{1 - (D_b/S) \cdot (D/L)}. \tag{19}$$

In order to minimize the quantity $D_b/m_0 g\eta$, the objective is to maximize r^{-1} or to minimize the Strouhal number by minimizing the overall drag-to-lift ratio D_b/S and by minimizing the wing drag-to-lift ratio D/L. The evolutionary pressure thus is to streamline the system body as well as the wing, a rather trivial but agreeable result. The minimization of $D_b/m_0 g\eta$ is considered an important evolutionary principle of sustained bird flight. Perusing the important survey of Strouhal number versus animal species presented in Figure 2 of [9], birds seem more successful in attaining small St than bats and insects in sustained flight.

In these considerations the question what constitutes the most desirable design cruise speed U_0 has not been explicitly addressed. It is known that travel speed increases weakly with animal size [9, 10].

It should be mentioned that some animals employ a combined down and forward stroke of their wings in sustained flight. Such a feature can also be incorporated into the oscillating wing model by adding a forward velocity component u_0 of the wing such that $\tan \varphi_0 = r^{-1} = (U_0 + u_0)/v_0$, $U_r = [(U_0 + u_0)^2 + v_0^2]^{1/2}$, $St = 2h_a f/U_0 = v_0/U_0 = (r^{-1} - u_0/v_0)^{-1}$. With these modifications, performance analysis proceeds as before, with no obvious aerodynamic advantages or disadvantages of this flight mode discernible.

4 SOME CURRENT ISSUES OF ANIMAL FLIGHT

4.1 Aero-wing with equal upstroke and downstroke duration (half-cycle thruster)

The oscillating aero-wing model as presented in Sections 1–3 neglected upstroke time compared to the lift and thrust generating downstroke duration, which does not conform to actual bird propulsion. Such a restriction can easily be relaxed with only minor modifications in analysis.

For instance, assume the noncontributing upstroke takes the same time as the lift and thrust force generating downstroke, as may be approximately the case for many animals. In this example, for the wing to generate the same average lift and thrust as a wing whose downstroke takes up most of the duration of a cycle, the wing needs to deliver twice as much lift and thrust during the downstroke half-cycle. Since the thrust-to-lift ratio remains the same, m and r^{-1} remain the same in half-cycle thrusting as in full-cycle thrusting. This means that the half-cycle thruster needs a wing with twice the surface area, preferably with aspect ratio and pitch angle α_0 unchanged.

A doubling in wing area needed for the half-cycle thruster compared to the full-cycle thruster seems to be disadvantageous, but in proper design the wing pitch angle α_0 can be kept the same in upstroke and downstroke and the wing experiences less severe accelerations during pitch reversals. These may be decisive operational advantages. Furthermore, since in the half-cycle thruster we need to add the half-cycle time of upstroking, the frequency of the cycle is lowered to half of the full-cycle thruster, i.e.

$$f = \frac{v_0}{4h_a} \tag{20}$$

and thus

$$St = \frac{1}{2r^{-1}}. \tag{21}$$

Neglecting the small forces in upstroke aerodynamics as before, the performance analysis of Section 3 also applies to the half-cycle thruster and would apply to a three-quarter-cycle thruster and to others as well. The half-cycle thruster in tandem with another 180° out-of-phase thruster, as in four-winged insects, should provide particularly smooth flying.

4.2 A criterion for quasi-steadiness in oscillating wing propulsion

Quasi-steadiness of oscillating wing propulsion may be expected if the distance d of adjacent vortices shed at stroke reversals is considerably larger than the wing chord length c. Translated into a formula, we need for quasi-steadiness of the half-cycle thruster:

$$\frac{d}{c} = \frac{\sqrt{(2h_a)^2 + (U_0/2f)^2}}{c} = \frac{2h_a}{c}\sqrt{1 + r^{-2}} \gg 1. \tag{22}$$

In our previous example in Section 3, $r^{-1} = 5$, thus the criterion (22) yields in case $h_a/c = 1$

$$\frac{d}{c} = 10.2\frac{h_a}{c} = 10.2 \gg 1. \tag{23}$$

Therefore, this benchmark example yields a quasi-steady situation. Birds seem to fall into this category during sustained travel. In contrast, consider a tethered fish [11] for which $r^{-1} = 0$, $h_a/c \simeq 1$ and thus $d/c = 2h_a/c \simeq 2$. This is an unsteady situation. For a traveling fish $r^{-1} = 1$, thus $d/c = 2.8$, still in the unsteady domain.

4.3 Flapping versus oscillating wings

Birds and insects operate by flapping and simultaneously pitching wings instead of a wing in simultaneous plunge and pitch, which we considered as a reference model. How compatible or similar are these modes of sustained propulsion? This question has recently been posed in the context of dragonfly flight [12]. A major result from their visualizations has been that the vortex, which develops behind the leading edge of a flapping wing pair during their simultaneous downstroke, is connected across the wing roots over the dragonfly body. This is similar as for the downstroke of a single wing in plunge as also visualized by them. This similarity of flapping and pitching wing aerodynamics should extend to symmetric flapping of other flying animals with wings not tapered toward the wing roots. For insects with strong taper toward the wing root, an oscillating wing pair model would be a better reference of comparison.

4.4 Wing tip vortices

The vortex structure near wing tips has recently been considered to be controversial [12] in the context of dragonflies [12] and butterflies [13] and by inference in the context of rectangular wings as well [12], the opposing view [14] receiving criticism. Smoke wire visualizations were at the core of both views and in [12] topological principles were used to bolster their view further. In essence, in [12, 13] the development of a leading edge vortex spanning the entire wing pair, then near the wing tips turning smoothly backward as tip vortices, has been postulated for the downstroke of dragonflies and butterflies which then gets shed during the upstroke. This vortex system has a nearly constant cross section. The diametrically opposite view [14] postulated a leading edge vortex turning forward near the wing tip and ending in a cone with the apex set on the wing tip. The backward oriented wing tip vortex also turned into a cone with the apex at or near that of the leading edge vortex. These results were obtained for a one-sided flapper modeled in the shape of a dragonfly wing during the downstroke, and then the vortex system was somehow swept downstream during the upstroke. It has been recognized [15, 16] that it is notoriously difficult to reconstruct vortex structures near wing tips by means of smoke wire visualization. An alternative method of global vortex tagging by smoke in areas of vorticity production was therefore developed to visualize tip vortices more definitively [15–23]. These prior visualizations were not concerned with dragonfly flappers but with rectangular and otherwise shaped wing tips and with steady or accelerating flow. The wing or half-wing was either static or in pitch. These visualizations all yielded similar results and it seems they would also be similar for flappers; this is the reason to present a sampling of previous visualization results which may shed some light on the current controversy. This is done with the aid of several figures as follows.

Figure 2 shows the basic experimental setup for visualizing wing tip vortex structures in a wind tunnel test section with flow direction as indicated and with a wing tip protruding into the section from the

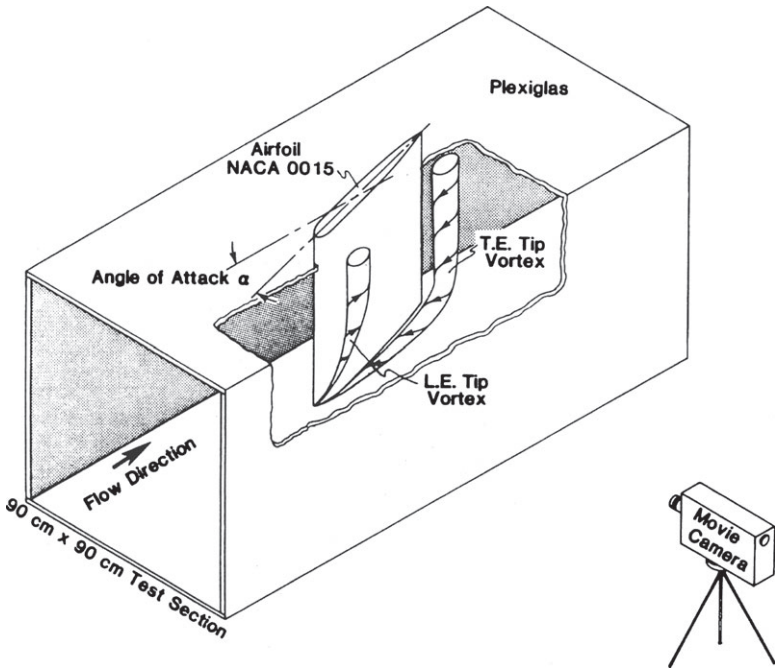

Figure 2: Three-dimensional sketch of the experimental setup for global vortex visualization.

top or with an entire wing mounted on thin wires in the tunnel at a desired geometric angle of attack. Flow can be steady or accelerating from rest. To visualize the vortex structure globally (in contrast to a cross-sectional cut obtainable by smoke wire visualization) liquid titanium tetrachloride is introduced as the smoke generating agent near the periphery of the wing where vorticity is generated, thus tagging the vortex structure with highly visible smoke. The flow is then filmed with a movie camera from outside the tunnel as sketched in Fig. 2 and more detail is provided in [17].

Figure 3 shows an assortment of four snapshots from movie sequences which show insightful wing tip vortex structures in a variety of flow configurations. Detailed sequences of vortex structure development and detailed data documentation for them are not provided here but are available in the references given in the figure caption. The top left sequence in Fig. 3 shows the vortex structure for a rectangular wing in steady flow at a 10° geometric angle of attack; the view is at the suction side of the wing. The nearly horizontally oriented tip vortices at the top and bottom wing tips, which are conical with apexes at the front corners of the wing, are visible. The separating boundary layer over the suction side of the wing is clearly separated from the conical tip vortices except at the front corners. The boundary layer decays into several vertical vortices which turn forward near the tip and also form cones with the apexes at the front corners. The formation of counterrotating cone pairs at each front corner is similar to what happens near the front corner of a delta wing and topologically corresponds to the structure A identified in [12] as typical for delta wings. The flow near the midsection of the wing near the leading edge is very two-dimensional; thus there is no location there

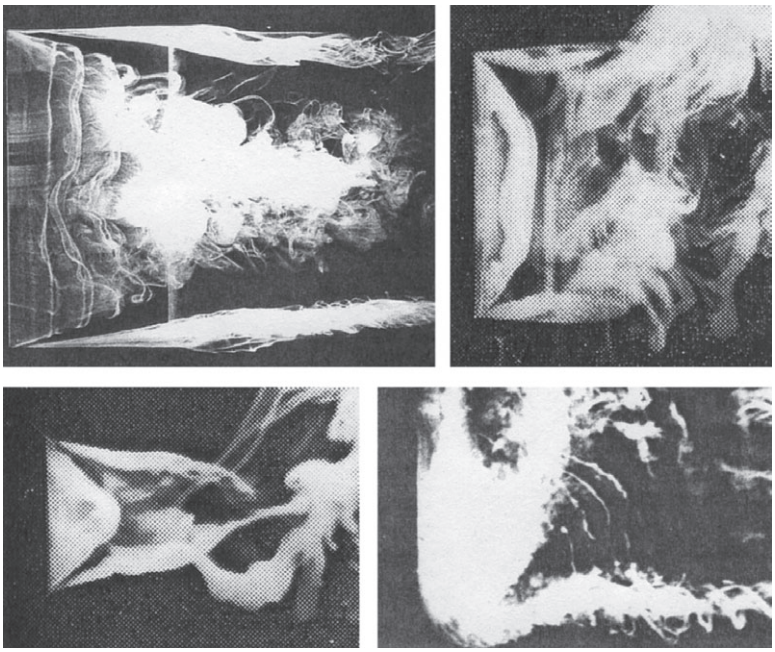

Figure 3: Upper left: Steady flow over a planar rectangular wing at 10° geometric angle of attack. From [20]. Upper right: Accelerating starting flow over a planar rectangular wing at 40° geometric angle of attack. From [16]. Lower left: Accelerating starting flow over a delta wing in reverse at 40° geometric angle of attack. From [16]. Lower right: Accelerating starting flow over a wing with a tip shaped as a semicircle at 40° geometric angle of attack. From [19].

for a three-dimensional structure termed by them C or U-shaped separation. Thus for the case at hand in the top left sequence in Fig. 3, the vortex structure is diametrically opposed to the structure conjectured in [12] for a flapping dragonfly wing pair and also conjectured by them to apply to a periodically plunging rectangular wing. Rather, the figure conforms to the view taken in [14].

The top right sequence in Fig. 3 shows accelerating starting flow over a rectangular wing at 40° geometric angle of attack shortly after start. Again we recognize the leading edge vortex turning conical and forward with the apex at the front corners, where the cones of the horizontal tip vortices also set anchor. The bottom left sequence in Fig. 3 shows a delta wing in reverse, i.e. the delta has its front corner backward, also exposed to starting flow at 40° geometric angle of attack. This shape corresponds somewhat to that of a butterfly wing pair. Again the leading edge vortex turns forward into cones which anchor at the front corners, as do the cones of the tip vortices which have slants rather than being horizontal. The bottom right sequence in Fig. 3 shows a half-wing protruding into the wind tunnel from the top and with a wing tip in the form of a semicircle, again in starting flow and at 40° geometric angle of attack. Again the leading edge vortex bends forward toward the lowest point of the tip vortex. There seems to be neckdown of the vortices near the tip but no apex can be clearly discerned there. An apex seems to require a well-defined corner rather than a well-rounded contour. In any case, all the examples exhibit the structures seen in [14] rather than the U-shaped separation seen in [12] and [13] for dragonflies and butterflies.

To somewhat reconcile the opposing views, consider Fig. 4, where an entire sequence of vortex development for a periodically pitching rectangular half-wing exposed to steady wind is shown for one oscillation period. Frames of the one period sequence are ordered into columns from top to bottom, then across columns from left to right. The sequence starts in the left most column with the downpitch to higher angle of attack. As the angle of attack increases a gap opens between counterrotating conical tip vortices anchored to the front corner of the rectangular wing tip, until the gap reaches maximum width in the second frame of the middle column. In the second half of the sequence during the pitchup with decreasing angle of attack, the gap between the counterrotating cones narrows until the cones mutually annihilate each other and the leading edge vortex connects directly backward into the trailing edge vortex while the vortex system gets swept away downstream. This construct in the late stage of leading edge vortex separation may be what has been seen in the context of dragonfly flapping in [12]. No U-shaped three-dimensional separation with a 3D critical point placed at the wing center or wing-pair center is required for this, i.e. the topological reasonings of [12] and [13] do not apply in this unsteady context. Topological arguments seem more tricky than originally envisioned.

5 CONCLUSIONS

An oscillating aero-wing model for use as a lifting thruster has been investigated in the quasi-steady domain. It is intended as a simple reference for sustained animal flight and MAVs. The propulsive efficiency of the model can be high, albeit the efficiency cannot be optimized with respect to the Strouhal number, in contrast to liftless propulsors in water. It is the streamlining of the systems body and of the wing which remain to minimize the energy consumption for flying. Some model refinements and current issues of oscillating wing propulsion have been addressed.

APPENDIX

Momentum theory of ideal propulsive efficiency η_{ideal} for aero-wing in the quasi-steady domain

Consider the control volume sketched in Fig. 5. The actuator disk area traced out by the wing is $A = 2h_a l$. Speed far upstream is U_0, at the disk u and far downstream there are components u_e and w_e in the horizontal and vertical directions as sketched. The atmospheric pressure is P_0 and the pressures

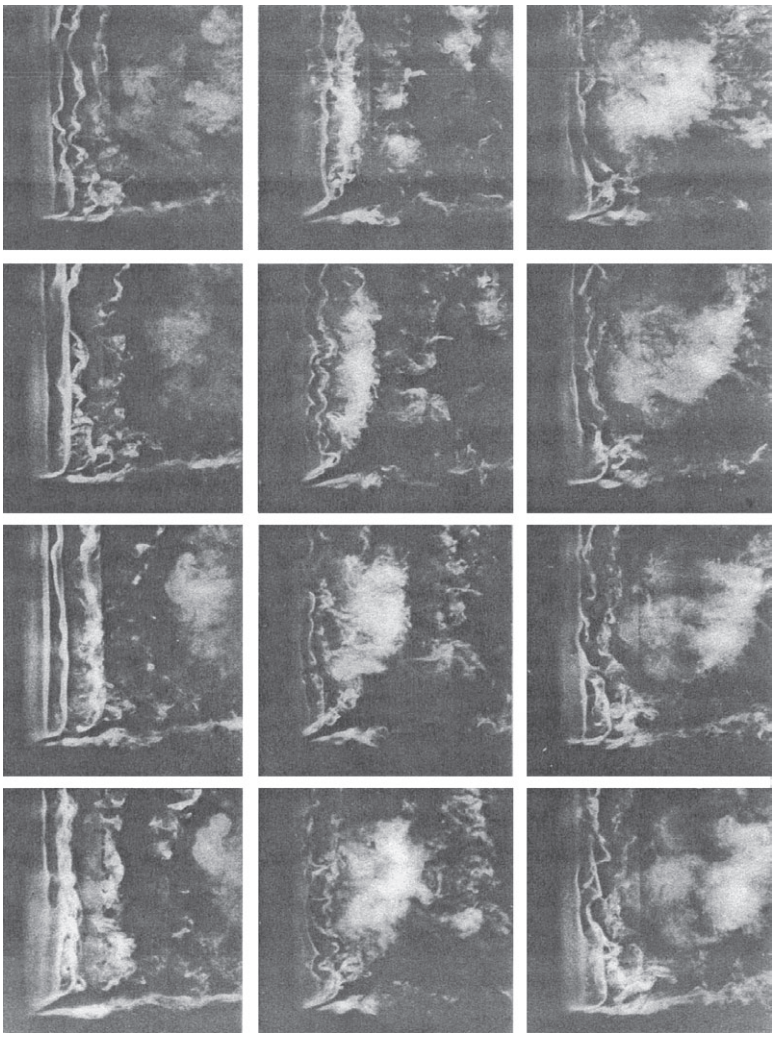

Figure 4: A rectangular half-wing in periodic pitch between 15° and 25° geometric angle of attack. From [15].

directly in front and behind the disk are P_i and P_e. Thrust and lift are

$$T = \dot{m}(u_e - U_0) \quad \text{and} \quad S = \dot{m}w_e, \qquad \text{where } \dot{m} = \rho A u,$$

$$w_e = \frac{S}{T}(u_e - U_0).$$

From Bernoulli:

$$\frac{\rho}{2}u^2 + P_i = \frac{\rho}{2}U_0^2 + P_0,$$

$$\frac{\rho}{2}u^2 + P_e = \frac{\rho}{2}(u_e^2 + w_e^2) + P_0.$$

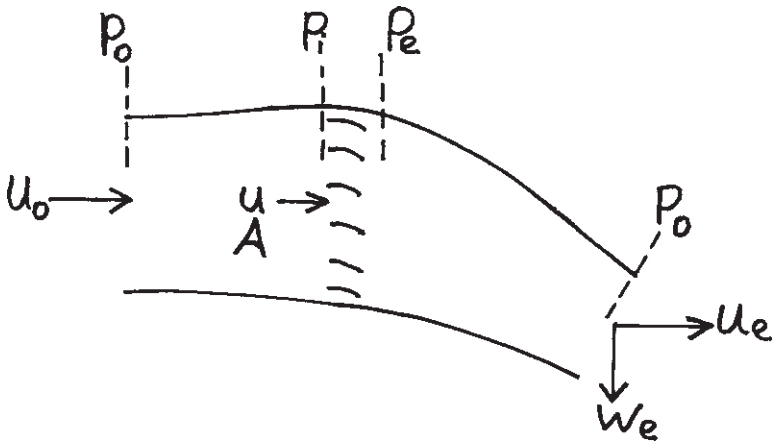

Figure 5: Sketch of control volume for incompressible and inviscid actuator disk theory for a wing propulsor with lift.

Thus by subtraction

$$P_e - P_i = \frac{\rho}{2}(u_e^2 + w_e^2 - U_0^2),$$

$$T = \rho A u(u_e - U_0) = (P_e - P_i)A = \frac{\rho A}{2}(u_e^2 - U_0^2 + w_e^2),$$

$$u = \frac{u_e + U_0}{2} + \frac{w_e^2}{2(u_e - U_0)} = \frac{u_e + U_0}{2} + \frac{u_e - U_0}{2}\frac{S^2}{T^2}$$

$$= U_0 + \frac{u_e - U_0}{2}\left(1 + \frac{S^2}{T^2}\right) = U_0 + \frac{T}{2\dot{m}}\left(1 + \frac{S^2}{T^2}\right).$$

Finding $\dot{m}$:

$$\dot{m} = \rho A u = \rho A U_0 + \frac{\rho}{2} A \frac{T}{\dot{m}}\left(1 + \frac{S^2}{T^2}\right),$$

$$\dot{m}^2 - \rho A U_0 \dot{m} - \frac{\rho}{2} A T\left(1 + \frac{S^2}{T^2}\right) = 0.$$

Thus

$$\dot{m} = \frac{\rho}{2} A U_0 + \sqrt{\left(\frac{\rho}{2} A u_0\right)^2 + \frac{\rho}{2} A T\left(1 + \frac{S^2}{T^2}\right)},$$

$$\dot{m} = \frac{\rho}{2} A U_0 \left[1 + \sqrt{1 + \frac{T}{(\rho/2)\, A U_0^2}\left(1 + \frac{S^2}{T^2}\right)}\right].$$

Introducing a thrust coefficient

$$C_A = \frac{T}{(\rho/2) A U_0^2},$$

we obtain

$$\dot{m} = \frac{\rho}{2} A U_0 \left[1 + \left(1 + C_A \left(1 + \frac{S^2}{T^2} \right) \right)^{1/2} \right].$$

We can now find the ideal propulsive efficiency

$$\eta_{\text{ideal}} = \frac{TU_0}{(\dot{m}/2)(u_e^2 - U_0^2 + w_e^2)} = \frac{TU_0}{(\dot{m}/2)(2T/\rho A)} = \frac{\rho A U_0}{\dot{m}};$$

inserting $\dot{m}$ from above yields

$$\eta_{\text{ideal}} = \frac{2}{1 + \sqrt{1 + C_A[1 + (S^2/T^2)]}}, \tag{*}$$

where we termed $S/T = m_0 g/D_b = m^{-1}$.

The propulsive efficiency becomes $\eta_{\text{ideal}} = 2/(1 + \sqrt{1 + C_A})$ in case $S/T = 0$, the well-known case of thrust without lift. Lift has a deteriorating effect on ideal efficiency. We still need to present C_A for the ideal case as follows. Note from eqn (14) when neglecting drag (D) (ideal case)

$$T = L \cos\varphi_0, \quad \text{where } \cos\varphi_0 = \frac{1}{\sqrt{1 + r^{-2}}}, \ \frac{S}{T} = r^{-1},$$

$$\frac{T}{(\rho/2) A U_0^2} = \frac{T}{(\rho/2) 2 h_a l U_0^2} = C_A = \frac{L}{(\rho/2) c l (U_0^2 + v_0^2)} \frac{c}{2h_a} \frac{U_0^2 + v_0^2}{U_0^2} \cos\varphi_0,$$

$$C_A = C_L \frac{c}{2h_a} \frac{\sqrt{1 + r^{-2}}}{r^{-2}}. \tag{**}$$

(*) in conjunction with (**) constitutes the ideal efficiency.

NOMENCLATURE

A	m^2	area of actuator disk (Fig. 5)
c	m	chord length of rectangular wing
C_A	–	thrust coefficient of actuator disk
C_D	–	drag coefficient of wing defined by eqn (10)
C_L	–	lift coefficient of wing defined by eqn (9)
d	m	distance of adjacent vortices
D	N	drag force of wing (Fig. 1)
D_b	N	drag force of animal or system body
f	s^{-1}	frequency of oscillating wing cycle
g	m s^{-2}	gravitational acceleration
h_a	m	lateral excursion of wing from mid-position
l	m	wing span
L	N	lift force of wing (Fig. 1)
m	–	ratio of thrust force to system weight (eqn (12))

m_0	kg	mass of system
$\dot{m}$	kg s^{-1}	mass flow across actuator disk (Fig. 5)
P_0	N m^{-2}	atmospheric pressure
P_e	N m^{-2}	pressure at downstream actuator disk surface (Fig. 5)
P_i	N m^{-2}	pressure at upstream actuator disk surface (Fig. 5)
r	–	inverse of r^{-1} (eqn (7))
r^{-1}	–	dimensionless travel speed (eqn (5))
Re	–	Reynolds number
S	N	lift of the animal or other system
St	–	Strouhal number (eqn (6))
T	N	thrust force of wing (Fig. 1)
u_0	m s^{-1}	forward velocity component of oscillating wing (usually $u_0 = 0$)
U_0	m s^{-1}	travel speed of animal or other system
u	m s^{-1}	speed at actuator disk (Fig. 5)
u_e	m s^{-1}	horizontal speed far behind actuator disk (Fig. 5)
v_0	m s^{-1}	lateral and constant downstroke speed of wing (Fig. 1)
w_e	m s^{-1}	lateral speed far behind actuator disk (Fig. 5)
α_0	deg or rad	pitch angle of wing (Fig. 1)
α_r	deg or rad	angle of attack of wing with the relative wind (eqn (8))
φ_0	deg or rad	angle of relative wind with the vertical (Fig. 1)
ρ	kg m^{-3}	density of air
ν	m^2 s^{-1}	kinematic viscosity
η	–	propulsive efficiency
$\eta_{\max}$	–	maximum propulsive efficiency
η_{ideal}	–	ideal propulsive efficiency according to momentum theory (Appendix)

REFERENCES

[1] Spedding, G.R., The aerodynamics of flight. *Mechanics of Animal Locomotion*, ed. R. Alexander, Springer-Verlag: Berlin, 1992.

[2] Freymuth, P., *Oscillating hydro-wing as a propulsor in the quasi-steady domain*. *Flow Phenomena in Nature*, ed. R. Liebe, WIT Press: Southampton, pp. 542–551, 2006.

[3] Weis-Fogh, T. & Jensen, M., Biology and physics of locust flight. 1. Basic principles in insect flight. A critical review. *Phil. Trans. Roy. Soc. B*, **239**, pp. 415–584, 1956.

[4] Jones, K.D., Lund, T.C. & Platzer, M.F., Experimental and computational investigation of flapping wing propulsion for micro air vehicles. *Prog. Astronautics and Aeronautics*, **195**, pp. 307–339, 2001.

[5] Hall, K.C. & Hall, S.R., A rational engineering analysis of the efficiency of flapping flight. *Prog. Astronautics and Aeronautics*, **195**, pp. 249–274, 2001.

[6] Anderson, J.M., Streitlien, K., Barrett, D.S. & Triantafyllon, M.S., Oscillating airfoils of high propulsive efficiency. *J. Fluid Mech.*, **360**, pp. 41–72, 1998.

[7] Kuethe, A.M. & Chow, C.Y., *Foundations of Aerodynamics*, 3rd edn, Wiley: New York, 1980.

[8] Holst, E. & Küchemann, D., Biologische und aerodynamische Probleme des Tierfluges, *Naturwiss.*, **29**, pp. 348–362, 1941.

[9] Taylor, G.K., Nudds, R.L. & Thomas, A.L.R., Flying and swimming animals cruise at a Strouhal number tuned for high power efficiency. *Nature*, **425**, pp. 707–711, 2003.

[10] Lighthill, J., Aerodynamic aspects of animal flight. *Swimming and Flying in Nature*, Vol. 2, eds. T.Y.T. Wu, C.J. Brokaw & C. Brennen, Plenum Press, pp. 423–491, 1975.

[11] Freymuth, P., Vortex visualizations for two-dimensional models of caudal fin fish propulsion. *Flow Phenomena in Nature*, ed. R. Liebe, WIT Press: Southampton, pp. 340–356, 2006.
[12] Thomas, A.L.R., Taylor, G.K., Srygley, R.B. & Nudds, R.L., Dragonfly flight: free-flight and tethered flow visualizations reveal a diverse array of unsteady lift-generating mechanisms, controlled primarily via angle of attack. *J. Exp. Biology*, **207**, pp. 4299–4323, 2004.
[13] Srygley, R.B. & Thomas, A.L.R., Unconventional lift-generating mechanisms in free-flying butterflies. *Nature*, **420**, pp. 660–664, 2002.
[14] Saharon, D. & Luttges, M.W., Three-dimensional flow produced by a pitching-plunging model dragonfly wing, Paper AIAA 87-0121, 1987.
[15] Freymuth, P., Finaish, F. & Bank, W., Visualization of wing tip vortices in unsteady and steady wind, Paper AIAA-86-1096, 1986. Also *AIAA J. Aircraft*, **23**, pp. 730–733, 1986.
[16] Freymuth, P. Finaish, F. & Bank, W., Further visualization of combined wing tip and starting vortex systems. *AIAA Journal*, **25**, pp. 1153–1159, 1987.
[17] Freymuth, P., Finaish, F. & Bank, W., The wing tip vortex system in a starting flow. *Zeitschrift für Flugwiss. Weltraumforsch.*, **10**, pp. 116–118, 1986.
[18] Freymuth, P., Visualizing the combined system of wing tip and starting vortices. *TSI Flow Lines*, Premier Issue, May 1986.
[19] Freymuth, P., Finaish, F. & Bank, W., Parametric exploration of unsteady wing tip vortices. *Flow Visualization IV*, Hemisphere Publishing Corp.: Washington, DC, pp. 419–424, 1987.
[20] Freymuth, P., Vortex topology of rectangular wings in pictures, sketches, and conjectures. *Journal of Flow Visualization and Image Processing*, **1**, pp. 1–13, 1993. Also *TSI Flow Lines* **6(1)**, pp. 9–13, 1991.
[21] Freymuth, P., Visualizing the connectivity of vortex systems for pitching wings, AIAA Paper 88-3549-CP, 1988. Also *Journal of Fluids Engineering (ASME)*, **111**, pp. 217–220, 1988.
[22] Freymuth, P., Vortex visualization as a reference for computer simulation. *Vortex Methods and Vortex Motion*, eds. K.E. Gustafson, & J.S. Sethian, SIAM: Philadelphia, PA, pp. 65–94, 1991.
[23] Freymuth, P., Flow visualization in fluid mechanics. *Rev. Sci. Instrum.*, **64**, pp. 1–18, 1993.